Investigation of the Nuclear Surface by Means of the Elastic Scattering of Heavy Ions*†

J. A. McIntyre, S. D. Baker,‡ and K. H. Wang
Yale University, New Haven, Connecticut

(Received September 5, 1961)

An investigation has been made to determine the relevant parameters in the elastic scattering of alpha particles and heavy ions by nuclei. First, it has been shown by the analysis of typical alpha-particle scattering data that the qualitative features of the scattering are determined by two parameters: (a) the strength of the Coulomb interaction and (b) the radius of the ion-nucleus interaction. Second, two experiments with different nuclei have been performed where the above two parameters were kept fixed in order to determine whether differences in the scattering would appear due to a third parameter, say, the nuclear surface thickness. To enhance the differences between the two experiments two doubly-magic nuclei, O^{16} and Pb^{208}, were used in the first scattering experiment while two aspherical nuclei, F^{19} and Tb^{159}, were used in the second scattering experiment. Differences in the scattering did occur between the two experiments. However, it is not possible to conclude that the differences are due to nuclear surface effects because of the inclusion of inelastic scattering in the data taken in the second experiment. An indication that there is not a difference between the "surfaces" of the Pb^{208} and Tb^{159} nuclei has been shown by making a partial-wave analysis of data taken by Yntema of the elastic scattering of alpha particles by these same nuclei.

I. INTRODUCTION AND SUMMARY

DURING the last five or six years a considerable number of experiments has been performed[1] concerning the elastic scattering of alpha particles and other heavy ions[2] from various target nuclei. The motivation for these experiments has been to obtain new information about the structure of nuclei. Work on alpha-particle scattering has shown already that the alpha particles that undergo scattering have penetrated very little into the nucleus. The success of the Blair sharp-cutoff approximation,[3] which assumes complete absorption of alpha particles striking the nucleus, and the optical-model calculations of Igo,[4] which show that only the outer edge of the optical potential affects the alpha-particle scattering, are typical results indicating that elastic scattering depends mainly on conditions at the nuclear surface. Study of the scattering of heavier ions has shown similar results.[1] The elastic scattering of heavy ions, therefore, presents a mechanism that may be used to investigate the nuclear surface in contrast to the mechanisms of electron and nucleon scattering which depend on the entire volume of the nucleus under study. A careful study of nuclei by elastically scattering heavy ions is therefore of considerable interest.

The first parameter determined by heavy-ion elastic scattering is a radius of interaction between the ion and the target nucleus. Systematic investigations with alpha particles of such radii over a range of nuclei throughout the periodic table by Kerlee *et al.*[5] and by Igo *et al.*[6] have shown that the interaction radius R' follows closely the relation: $R'=r_0A^{\frac{1}{3}}+r_a$ where r_0 is a constant and r_a is another constant, presumably the radius of the alpha particle. In particular, the interaction does not seem to be sensitive to nuclear structure effects such as closed shells as was noted by Kerlee *et al.*[5] A second parameter, a "surface thickness" (the region where the ion interacts with the nuclear potential and yet still can escape from the nucleus) can also be determined by heavy-ion scattering.[1] Very little work has been done to determine how this parameter changes among the various nuclei; the three nuclei studied by Igo[4] revealed the same "surface thickness."

The purpose of this paper is twofold. First, the physical parameters dominating the elastic scattering are exhibited. This is accomplished by showing in Sec. II.B that the qualitative features found in elastic scattering experimental data can be reproduced by adjusting two parameters in the scattering phase-shift analysis outlined in Sec. II.A. These two parameters are $\eta=ZZ'e^2/\hbar v$, the Coulomb interaction strength parameter, and R', the interaction radius of the nucleus and the scattered ion.

The second purpose of this work is to eliminate experimentally the effects of the two dominant parameters so that the smaller effects of other parameters can be exhibited. This purpose is accomplished by performing two experiments in which η and L', the partial wave number associated with the nuclear radius R', are unchanged (see Sec. III.A). Any difference in the scattering would then be caused by some nuclear parameter other than η and R', the difference being

* Work supported by the U. S. Atomic Energy Commission.

† Preliminary reports of different portions of this work have been recorded in *Proceedings of the Second Conference on Reactions between Complex Nuclei*, edited by A. Zucker, E. C. Halbert, and F. T. Howard (John Wiley & Sons, Inc., New York, 1960), p. 180, and in *Proceedings of the International Conference on Nuclear Structure*, edited by D. A. Bromley and E. W. Vogt (Toronto University Press), p. 384.

‡ Raytheon Predoctoral Fellow in Physics, 1960–1961.

[1] R. M. Eisberg and C. E. Porter, Revs. Modern Phys. **33**, 190 (1961); this paper reviews alpha-particle scattering. A. Zucker, Ann. Rev. Nuc. Sci. **10**, 27 (1960); this paper reviews heavy-ion scattering.

[2] In this paper, to avoid confusion in describing interactions, the bombarding nucleus (including the alpha particle) will be called a heavy ion and the target nucleus a nucleus.

[3] J. S. Blair, Phys. Rev. **95**, 1218 (1954).

[4] G. Igo, Phys. Rev. Letters **1**, 72 (1958); Phys. Rev. **115**, 1665 (1959).

[5] D. D. Kerlee, J. S. Blair, and G. W. Farwell, Phys. Rev. **107**, 1343 (1957).

[6] G. Igo, H. E. Wegner, and R. M. Eisberg, Phys. Rev. **101**, 1508 (1956).

caused very likely by conditions at the nuclear surface, since this is the region where the main interaction occurs. However, the effects on the scattering of a spin-orbit interaction or of a nuclear polarization by the heavy ions, for example, may not be negligible. In order to enhance the effect of surface differences the two scattering experiments were performed with ions and nuclei as dissimilar as possible (see Sec. III.B). In the first experiment O^{16} ions were scattered from Pb^{208} nuclei (both nuclei being doubly-magic and hence spherical) while in the second experiment F^{19} ions were scattered from Tb^{159} nuclei (both nuclei being aspherical).

The experimental results do, indeed, show a difference between the two experiments (Sec. III.C). However, it has not been possible to eliminate the inelastic scattering contribution in the ($F^{19}+Tb^{159}$) experiment. The magnitude of this contribution (assuming it to be due to Coulomb excitation) is comparable to the difference found between the two experiments and so it is unclear whether a difference in the elastic scattering actually occurs.

In order to throw some light on the magnitude of the effect of the inelastic scattering in the ($F^{19}+Tb^{159}$) experiment, we asked J. L. Yntema at the Argonne National Laboratory to measure the elastic scattering of alpha particles by Pb^{208} and Tb^{159} at approximately the same projectile velocity as the experiments with O^{16} and F^{19}. With the smaller-charged alpha particles, the inelastic scattering (Coulomb excitation) was reduced to a few percent of the elastic scattering. A partial-wave analysis of the alpha-particle experimental data taken by Yntema, Zeidman, and Braid at Argonne revealed no difference between the Pb^{208} and Tb^{159} nuclei aside from their radii. This result is an indication then that the Pb^{208} and Tb^{159} "surfaces" are the same and that the difference between the scattering results for Pb^{208} and Tb^{159} with the heavier ions is caused by the inclusion of inelastic scattering in the ($F^{19}+Tb^{159}$) experiment or by some neglected effect such as a spin-orbit interaction or a nuclear polarization by the heavy ion.

II. DETERMINATION OF THE PARAMETERS RESPONSIBLE FOR SCATTERING

A. Method of Analysis

A procedure that is useful for analyzing heavy-ion scattering is a semiclassical partial wave approximation.[3,7,8] The scattered ions are described by partial waves and the nucleus is assumed to be strongly absorbing. Use is made of the fact that the Lth partial wave has a small amplitude inside the radius R, where R is related to the angular momentum $L\hbar$ by the semiclassical expression:

$$L(L+1)=\rho(\rho-2\eta), \tag{1}$$

with

$$\rho=R/\lambda\!\!\!^{-}. \tag{2}$$

Here, $2\pi\lambda\!\!\!^{-}$ is the de Broglie wavelength of the ion at infinity in the center-of-mass system, while

$$\eta=ZZ'e^2/\hbar v \tag{3}$$

is the Coulomb field parameter (Ze and $Z'e$ are the charge on the nucleus and the ion, respectively, $2\pi\hbar$ is Planck's constant, and v is the relative velocity of the ion and the nucleus). Because of the small amplitude of the Lth partial wave inside of R, an absorbing nucleus of radius R' will attenuate strongly partial waves with L values less than L', where L' is determined from $R'=\rho'\lambda\!\!\!^{-}$ by use of Eq. 1.

In the Blair sharp-cutoff approximation,[3] the amplitudes of the partial waves are reduced from full value to zero at the L' corresponding to the nuclear radius R'. In the work to be presented here, the transition from no attenuation to complete attenuation will be made less sharp by using the following arbitrary expression for the amplitude A_L of the Lth partial wave[8]:

$$A_L=\{1+\exp[-(L-L')/\Delta L_A]\}^{-1}. \tag{4}$$

A plot of A_L against L is given in Fig. 1. Two variables are seen to determine A_L in Eq. (4): (1) L' is the partial-wave number corresponding to the nuclear radius R' (for this partial wave, $A_L=\frac{1}{2}$) and (2) ΔL_A is a measure of the number of partial waves over which the transition from zero to complete attenuation of the partial waves occurs. Just as L' can be related semiclassically to a nuclear "radius" R', so can ΔL_A be related to a nuclear "surface thickness" ΔR. Differentiation of Eq. (1) gives the relation between ΔL_A

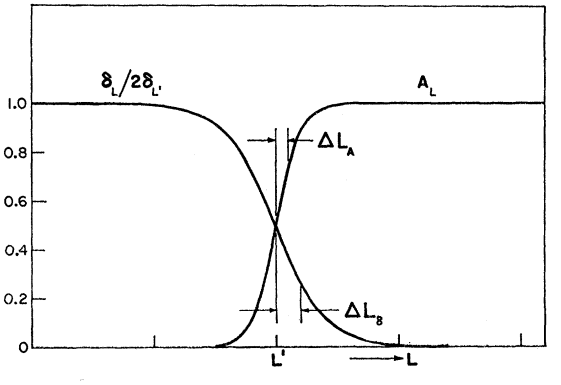

FIG. 1. The amplitude of the Lth partial wave, A_L, plotted against L as is also the nuclear phase shift, δ_L (normalized to $2\delta_{L'}$). For $L=L'$, $A_L=\frac{1}{2}$ and $\delta_L=\delta_{L'}$. ΔL_A and ΔL_δ are parameters determining the range of L over which A_L and δ_L drop from their maximum values to zero.

[7] J. E. Turner, J. S. McIntosh, and S. C. Park, Bull. Am. Phys. Soc. 3, 223 (1958); J. S. McIntosh, S. C. Park, and J. E. Turner, Phys. Rev. 117, 1284 (1960).

[8] J. A. McIntyre, K. H. Wang, and L. C. Becker, Phys. Rev. 117, 1337 (1960).

and ΔR as follows:

$$(2L+1)\Delta L_A = 2\rho(\rho-\eta)\Delta R/R. \quad (5)$$

In addition to an attenuation of the partial waves, earlier work has shown[8] the necessity for introducing an additional phase shift into the partial waves due to the effect of the nuclear potential on the scattering. This nuclear phase shift will vanish for large-L partial waves which do not approach the nucleus and will increase as the L value is decreased. For partial waves with L values corresponding to an R value considerably less than R', the absorption radius, the nuclear phase shift is irrelevant because these partial waves are completely attenuated. A convenient but arbitrary expression for the nuclear phase shift that satisfies these conditions is[8]

$$\delta_L = 2\delta_{L'}\{1+\exp[(L-L')/\Delta L_\delta]\}^{-1}. \quad (6)$$

A plot of this function is shown also in Fig. 1. Three variables determine δ_L in Eq. (6): (1) L', corresponding to the nuclear radius R', is the same parameter as the L' used above in the expression for A_L, (2) ΔL_δ is a measure of the number of partial waves over which the transition from zero to maximum nuclear phase shift occurs, and (3) $\delta_{L'}$ is the strength of the nuclear phase shift at $L=L'$ and so is a measure of the depth of the nuclear potential at R'.

The differential cross section σ for the scattering of an ion of charge $Z'e$ by a nucleus of charge Ze may then be expressed in terms of A_L, δ_L, and the Coulomb partial waves. A convenient expression is found by subtracting the attenuated partial waves from the scattering for all of the partial waves[3,9]:

$$\sigma/\sigma_R = |-i\exp[-i\eta\ln(\sin^2(\theta/2)] - \eta^{-1}\sin^2(\theta/2)\sum_{L=0}^{\infty}[1-A_L\exp(2i\delta_L)](2L+1) \times P_L\exp[2i(\sigma_L-\sigma_0)]|^2. \quad (7)$$

Here σ_R is the Rutherford scattering differential cross section, θ is the scattering angle in the center-of-mass system, η is given by Eq. (3), P_L is the Lth Legendre polynomial, and σ_L is the Coulomb phase shift, where

$$\sigma_L-\sigma_{L-1}=\tan^{-1}(\eta/L). \quad (8)$$

The effect of the nucleus on the scattering is introduced through A_L and δ_L as given in Eqs. (4) and (6).

B. Analysis of Experiments

A review of the many experimental angular distributions that have been published reveals striking differences in the qualitative aspects of these distributions. The question which naturally arises then is: "What is the relationship between the scattering features and the structure of the nucleus that causes the scattering?" The purpose of this section is to use the description of the scattering outlined in the previous section to calculate (using an IBM 650 computer) how changes in the nucleus will affect the scattering results.

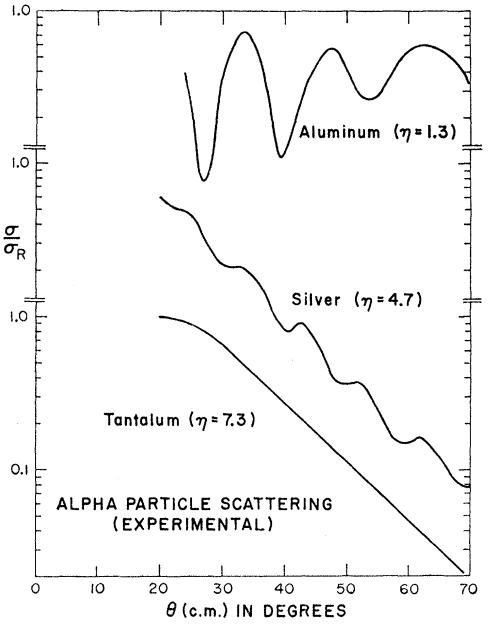

FIG. 2. Experimental angular distributions of alpha-particle elastic scattering. The differential scattering cross section σ is divided by the Rutherford scattering cross section σ_R and plotted against the center-of-mass scattering angle.

A qualitative summary of the angular distributions obtained experimentally by heavy-ion scattering is shown in Fig. 2. The three distributions shown are taken from a paper of Igo *et al.*[6] which reports the experimental results obtained for the scattering of 40-Mev alpha particles. In the figure, the ordinate is the differential cross section σ divided by the Rutherford differential cross section σ_R, while the abscissa is the center-of-mass scattering angle θ. Almost all of the heavy-ion scattering data published to date[10] can be classified according to one of the three curves shown in Fig. 2: (1) large oscillations (Al curve), (2) a drop in cross section with wiggles (Ag curve), and (3) a smooth drop in cross section (Ta curve). From an experimental point of view it is important to determine whether these large qualitative differences are the result of nuclear structure differences among the various nuclei. If nuclear structure effects can be shown to be responsible for these differences, then rather rough experiments will suffice for a study of nuclear structure effects.

To test whether the qualitative differences in scattering shown in Fig. 2 reveal any effects of nuclear

[9] N. F. Mott and H. S. W. Massey, *The Theory of Atomic Collisions* (Clarendon Press, Oxford, 1949), 2nd ed.

[10] Excluded in this discussion are scattering data from resonance-type interactions such as those studied by D. A. Bromley, J. A. Kuehner, and E. Almqvist, Phys. Rev. Letters 4, 365 (1960).

structure three calculations were made to determine the scattering from three hypothetical nuclei which were given the same nuclear structure but for which the three scattering conditions (the value for η) were different. The nuclear parameters chosen for all three nuclei were: $R'=9.22\times10^{-13}$ cm and $\Delta R_A/R'=0.0434$. (The R' and $\Delta R_A/R'$ values were chosen to be those found earlier to fit the 40-Mev alpha-particle scattering from Ag.[8]) For simplicity, the effects of the nuclear potential were assumed to be zero so that the δ_L's, the nuclear phase shifts, were set equal to zero. Application of Eqs. (1) and (5) then yielded values for L' and ΔL_A for each of the three values of η, which were chosen to be the same as the values shown in Fig. 2. (L' and ΔL_A were calculated for 40-Mev alpha particles taking into account the recoil of the target nucleus.) Equation (4) then permitted the calculation of A_L for each of the three pairs of L' and ΔL_A. Use of Eq. (7) then gave σ/σ_R, the ratio of the scattering cross section to Rutherford scattering. The ratios obtained by these calculations are plotted in Fig. 3. Inspection of Fig. 3 shows that the *qualitative* features of Fig. 2 have been reproduced, i.e., oscillations for $\eta=1.3$, wiggles for $\eta=4.7$, and a smooth drop for $\eta=7.3$. The conclusion is, therefore, that the large experimental qualitative differences in Fig. 2 result from the changes in the value of η and not from the structure of the nucleus. This

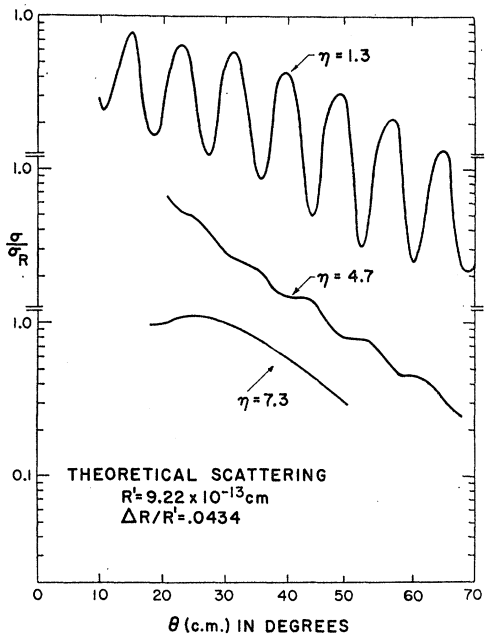

FIG. 3. Calculated angular distributions using the partial wave analysis described in Sec. II.A. The scattering parameters L' and ΔL_A were determined by setting $R'=9.22\times10^{-13}$ cm and $\Delta R/R'=0.0434$ for all three angular distributions and by changing only η as indicated. The same values for η were used as in Fig. 2. With these values of L' and ΔL_A, A_L was then determined, while δ_L was set equal to zero. A_L and δ_L then determined σ/σ_R.

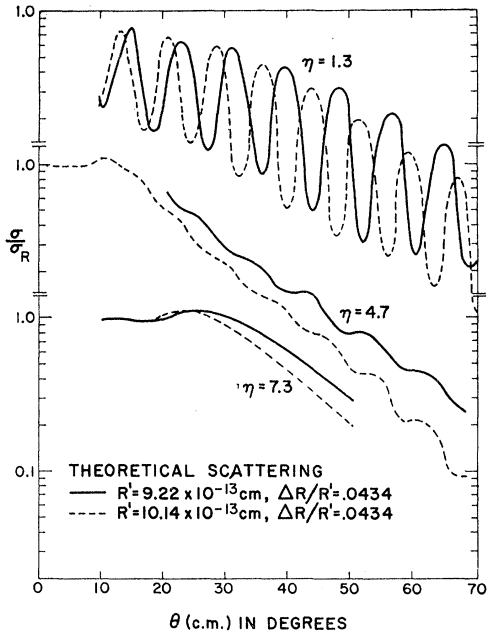

FIG. 4. The effect of a 10% increase in the nuclear radius R. The solid curves are the same as the curves in Fig. 3; the dashed curves correspond to a 10% increase in radius.

conclusion is in agreement with an earlier observation[11] that the transition from the oscillatory-type angular distribution to the smooth drop-off type occurs for η values of about 5, independent of the nuclei involved in the scattering, showing thereby that η is the dominating parameter.

In order to determine the effect of the nuclear radius on the scattering, a second calculation was made to find the effect of a change in the nuclear radius. The value for R' was increased by 10% to be 10.14×10^{-13} cm, $\Delta R_A/R'$ was kept at 0.0434, and the δ_L's kept at zero. σ/σ_R was again calculated for the same three values of η. The results of the calculations are shown in Fig. 4 where the dashed lines are for the nucleus with the 10% larger radius and the solid lines are for the original nucleus (same curves as in Fig. 3). The effect of a 10% change in radius is clearly seen: in the $\eta=1.3$ case the oscillation period is changed by about 10% while in the $\eta=7.3$ case the angle at which the drop below Rutherford scattering occurs has been changed about 10%. Both phenomena have been used in the past to determine nuclear radii.[1] However, as discussed in the Introduction, the nuclear radii have been found to follow quite closely the $A^{\frac{1}{3}}$ law[5,6] so that the determination of nuclear radii has not yet yielded any information about nuclear structure. Also, it is interesting that a change in the nuclear radius does not affect the amplitude of the oscillations on the angular distribution curves. This feature again is in agreement

[11] J. A. McIntyre, S. D. Baker, and T. L. Watts, Phys. Rev. 116, 1212 (1959).

with the observation[11] that these oscillations depend chiefly on the value of η.

The next step in investigating the effects of the nuclear parameters would seem to be to calculate the effect of changing the nuclear "surface thickness" ΔR_A. However, as has been noted in the Introduction, no effects of such changes in nuclear structure have as yet been detected so that the question which really needs to be answered is whether an experimental effect independent of η and R' can be isolated. It is for this reason that, at this point, the calculational procedure is laid aside and an experimental attack is made on the problem.

III. AN EXPERIMENT TO DETERMINE THE MAGNITUDE OF "SURFACE" EFFECTS

A. Theoretical Foundation

It will now be shown that it is possible to perform scattering experiments between different heavy ions and nuclei such that η and L' do not change for the different pairs of ions and nuclei. Since η determines the Coulomb interaction while L' determines the nuclear radius, any difference between the results of such experiments must be assigned to changes in parameters other than the Coulomb interaction and the nuclear radius. These changes presumably indicate changes at the nuclear surface because the strong absorption by the nucleus prohibits the scattered ions from penetrating into the nucleus, although other effects such as spin-orbit interactions are by no means excluded. It is interesting to note that all of the scattering experiments performed with the same η and L' would be described by one Blair sharp-cutoff curve since the only parameters in the sharp-cutoff approximation are η and L'.

There are five variables that may be adjusted experimentally:

$$Z,\quad A,\quad Z',\quad A',\quad v, \tag{9}$$

where Z and Z' are the atomic numbers of the nucleus and ion, respectively, A and A' are the corresponding atomic weights, and v is the relative velocity of the ion and the nucleus. Two constraints exist because of the fixed relation between the atomic number Z and the atomic weight A:

$$A=A(Z), \tag{10a}$$

$$A'=A'(Z'), \tag{10b}$$

so that only three independent variables Z, Z', and v remain. By selecting a value for η, one more independent variable is removed, say v. Finally the choice of a value for L' introduces a relation between Z and Z' so that Z may be expressed as a function of Z' and the two selected parameters, η and L':

$$Z=Z(Z',\eta,L'). \tag{11}$$

Equation (11) shows that for chosen values of η and L', there is a fixed value of Z (the target nucleus charge number) for each value of Z' (the ion charge number). Thus a range of target nuclei can be studied without changing η and L', providing that the correct adjustment is made in the identity of the bombarding ion.

The procedure followed then was to perform two scattering experiments chosen to maximize differences in nuclear structure. The first experiment was the scattering of O^{16} by Pb^{208}. Both of these nuclei are doubly-magic and hence are spherical. The second experiment was the scattering of F^{19} by Tb^{159}. Both of these nuclei are aspherical and Tb^{159} is known to have an ellipsoidal shape with the major axis approximately 30% larger than the minor axis.[12] The "nuclear surface" for Tb^{159} nuclei randomly oriented in the target would therefore be expected to be much "fuzzier" than that for the doubly-magic Pb^{208} nucleus. Unfortunately the constraints are such that Tb^{159} and Pb^{208} cannot both be studied with O^{16} ions if η and L' are to be kept unchanged. However, for the problem at hand—the determination whether or not a nuclear surface effect can be detected—whatever asphericity there is for the F^{19} nucleus contributes so as to enhance the effect being sought.

The ($O^{16}+Pb^{208}$) experiment was performed at the maximum ion energy available while the ($F^{19}+Tb^{159}$) experiment was performed with a degraded F^{19} beam so that η and L' were approximately the same for each experiment. The values of the various parameters are summarized in Table I. Exact matching of η and L' cannot be obtained because the Z values available experimentally are integers whereas the Z values calculated from Eq. (11) are not. Also, a rare-earth mono-isotopic element was required for a clean experiment; this restriction further limited the Z-value possibilities. Notice also should be taken of an uncertainty in the determination of L' because of the uncertainty associated with the value of the nuclear radius R'. The first two R' values given in Table I (see column 5) were calculated using the relation $R'=r_0(A^{\frac{1}{3}}+A'^{\frac{1}{3}})$, with r_0 being chosen to be 1.47×10^{-13} (see column 4). This value for r_0 has been found by Reynolds *et al.*[13] to be consistent with a number of scattering experiments conducted with heavy ions. The third R' value shown in column 5 was calculated using a 3% larger r_0 value for the $F^{19}+Tb^{159}$ interaction radius (see column 4). An increase in r_0 for Tb^{159} of about 2% has been found by Kerlee, Blair, and Farwell[5] for alpha-particle scattering so that the correct value for R' for Tb^{159} probably lies between the two values shown. This change in R' corresponds to a change in L' from 89 to 93 (see column 6). The value for L' for the ($O^{16}+Pb^{208}$) experiment was 93 which lies in the range of L' values possible for ($F^{19}+Tb^{159}$). The values for η for the two experiments were almost identical since

[12] K. Alder, A. Bohr, T. Huus, B. Mottelson, and A. Winther, Revs. Modern Phys. 28, 432 (1956).

[13] H. L. Reynolds, E. Goldberg, and D. D. Kerlee, Phys. Rev. 119, 2009 (1960).

TABLE I. Summary of the experimental parameters.

Column	1	2	3	4	5	6	7
Parameter	E (Mev)	Z'	Z	r_0(est.) (10^{-13} cm)	R'(est.) (10^{-13} cm)	L'(est.)	η
$O^{16}+Pb^{208}$	157	8	82	1.47	12.40	93	31.75
$F^{19}+Tb^{159}$	142	9	65	1.47	11.89	89	31.85
				1.52	12.25	93	

the ion energy E could be adjusted smoothly; for ($O^{16}+Pb^{208}$), $\eta=31.75$, while for ($F^{19}+Tb^{159}$), $\eta=31.85$ (see column 7).

B. Experimental Apparatus

The beams of O^{16} and F^{19} ions used in the experiments were supplied by the Yale Heavy-Ion Accelerator. The beams were each deflected by a bending magnet which dispersed the ions of different energy; a slit in the dispersed beam then defined the energy spread of the beam. The energy-analyzed beam was again deflected to be parallel to the initial beam and finally passed through a $\frac{1}{8}$-in. wide by $\frac{1}{4}$-in. high slit into the 8-in. diameter scattering chamber. Aluminum and beryllium foils near the second slit were used to degrade the beam energy to the desired value. Ions scattered by the target at the center of the scattering chamber were detected by a 0.010-in. thick by $1\frac{1}{2}$-in. diameter CsI(Tl) scintillator viewed by an EMI 9536-B photomultiplier,[14] the scintillator being glued to a $\frac{1}{4}$-in. thick Lucite disk of the same diameter as the scintillator.[15] The disk was coupled to the photomultiplier with Dow-Corning No. 200 Silicone Oil. The scintillation pulses were amplified and then analyzed by a RIDL 400-channel pulse-height analyzer.[16] A $\frac{1}{8}$-in. wide by $\frac{1}{4}$-in. high slit in front of the scintillator determined the solid angle of the detector. The detector was mounted on a remotely-controlled table rotating about the target, the detector being outside the scattering chamber and approximately 20 in. from the target. A 0.001-in. Mylar window, 1 in. high, encircled the scattering chamber from scattering angles of $-10°$ to $+160°$ so that the scattered ions could leave the scattering chamber; this range of angles permitted counting to be performed on both sides of the beam, the beam direction thereby being determined. An evacuated pipe extended from the scattering chamber to the scintillation counter, the entrance window to this pipe being made of 0.00125-in. Mylar. The counter angle with respect to the beam was read remotely to 0.01° by reading a scale with a television system. The Mylar window in the scattering chamber was protected from the ion beam by means of a cylindrical can mounted on an insulated bearing inside, and coaxial with, the scattering chamber. A hole was cut in the side of the can in the counter direction so that scattered ions could reach the counter from the target. A permanent magnet attached to the counter pipe rotated the can when the counter was rotated so that the hole in the can continued to lie between the counter and the target. A horizontal slot was also cut in the can so that the incoming ion beam would not be intercepted by the can. The can was used also for monitoring the beam, the ion charge collected on the can being transferred to a polystyrene capacitor; the capacitor voltage was measured with a Cary electrometer.[17] A positive 1000-v potential was applied to the target so that electrons knocked out of the target would not reach the can. Nevertheless, the can was not depended upon to give the absolute value of the ion current; rather, the scattering data were normalized to Rutherford scattering at the small scattering angles. Three target positions were available on the remotely controlled vertically moveable target holder. The Pb^{208} (98% pure) and the Tb^{159} (100% pure) targets were evaporated onto 50-μg/cm^2 Formvar films. The Pb^{208} foil was about 300 μg/cm^2 thick and the Tb^{159} foil about 600 μg/cm^2 thick.

The energy of the ion beam was determined by range measurements in aluminum. A thick aluminum target (25 mg/cm^2) was placed in the beam and the scintillation counter was set at a large angle ($\sim$40°) where elastic scattering was negligible so that mainly alpha particles and protons were detected. Using the can described above as a Faraday cup, additional aluminum foils were placed in the ion beam before the target until the ions could no longer penetrate the thick target and the Faraday cup reading dropped abruptly. The alpha-particle production in the aluminum target, on the other hand, would be expected to change only slightly over the small change of energy associated with the stopping of the beam in the target. Thus, the

[14] Two tubes of this type were tested for pulse-height resolution and were found to give 2.4% resolution (full width at half maximum) as compared to 3.3% for RCA 6292 photomultipliers for 8.8-Mev alpha particles. The tubes were obtained from H. L. Hoffman and Company, 35 Old County Road, Westbury, L. I., New York.

[15] Obtained from the Harshaw Chemical Company, Cleveland, Ohio.

[16] Radiation Instrument Development Laboratory, Inc., 61 East North Avenue, Northlake, Illinois.

[17] Cary Electrometer, Model 31, Applied Physics Corporation, Pasadena, Caifornlia.

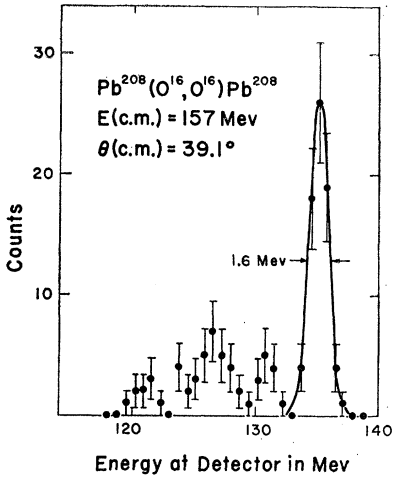

FIG. 5. Energy resolution obtained with the scintillation counter for the (O^{16}+Pb^{208}) scattering taken at 39.1°, the largest scattering angle.

counting rate of the scintillation counter could be used to monitor the Faraday cup reading. Using this technique, the extrapolated range of the ion beam was determined to ± 0.2 mg/cm^2. The beam energy was then calculated using the range-energy data of Northcliffe[18] which permitted a determination of the energy to ± 1 Mev.

Using the same analysis as that described for previous work,[11] the angular resolution (full width at half-maximum) was found to be 0.7° for the (O^{16}+Pb^{208}) experiment and 0.9° for the (F^{19}+Tb^{159}) experiment. The energy resolution of the system is shown in Figs. 5–7. The 1.6-Mev resolution shown in Fig. 5 for the (O^{16}+Pb^{208}) scattering is good enough to eliminate any inelastic scattering caused by exciting the lowest energy levels in Pb^{208} or O^{16} (2.6 Mev and 6.1 Mev, respectively). The energy resolution shown in Fig. 6 for the (F^{19}+Tb^{159}) scattering is not nearly good enough to discriminate against inelastic scattering caused by exciting the low-lying Tb^{159} and F^{19} levels (58 kev and 110 kev, respectively). However, the elastic scattering cross section is so large at the small angle of 11.2° ($\sim$10 barns/steradian) and the trajectory of the scattered ion passes at such a large distance from the nucleus (about three nuclear radii) that the scattering should be predominantly elastic. The peak width in Fig. 6 therefore is instrumental. It is larger than the width in Fig. 5 because the energy-selecting slits in the beam were opened up wider for the F^{19} beam than for the O^{16} beam to increase the F^{19} beam intensity and also because the F^{19} beam was degraded in energy by foils. At the largest scattering angles where inelastic scattering of other events would be more important a peak width such as that shown in Fig. 7 was obtained. The width is virtually the same as that obtained at small angles although small "tails" appear on both sides of the peak. These tails were assumed to indicate

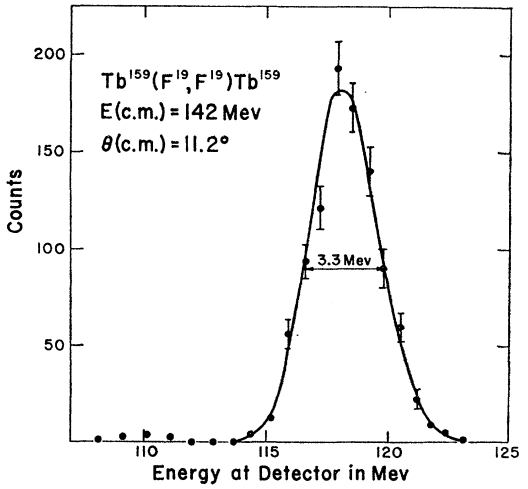

FIG. 6. Energy resolution obtained for the (F^{19}+Tb^{159}) scattering at a small (11.2°) scattering angle.

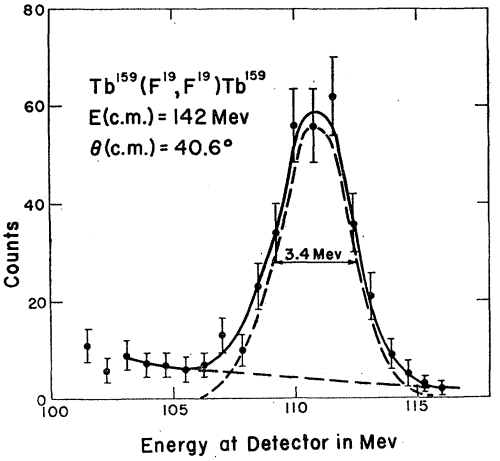

FIG. 7. Energy resolution obtained for the (F^{19}+Tb^{159}) scattering at 40.6°, the largest scattering angle.

a constant background under the peak. A subtraction was therefore made as shown in Fig. 7 and the dashed peak used to determine the scattering cross section. The scattering is not completely elastic at the larger scattering angles. For the range of scattering angles investigated the ratio of Coulomb excitation of the first level of Tb^{159} to Rutherford scattering[12] (assuming a point nucleus and a weak Coulomb interaction) is shown in Fig. 8. The Coulomb excitation is seen to contribute more than 10% to the scattering for scattering angles greater than 27°.

C. Experimental Results

The differential cross sections measured for (O^{16}+Pb^{208}) elastic scattering are shown in Fig. 9. The ordinate is the differential cross section σ divided by the Rutherford cross section σ_R where

$$\sigma_R = \{(ZZ'e^2/4E)\csc^2(\theta/2)\}^2. \quad (12)$$

[18] L. C. Northcliffe, Phys. Rev. 120, 1744 (1960).

Here, E is the energy and θ is the scattering angle in the center-of-mass system. The abscissa in Fig. 9 is the center-of-mass scattering angle. For comparison purposes, a Blair sharp cutoff curve calculated for $\eta=31.8$ and $L'=93$, the chosen experimental values for η and L' (see Table I), has also been plotted in Fig. 9. The curve fits the experimental data nicely until the cross section drops below the Rutherford value.

The $F^{19}+Tb^{159}$ data are shown in Fig. 10, the same data being plotted twice for comparison to different sharp-cutoff curves. The top sharp-cutoff curve was calculated for $\eta=31.8$ and $L'=93$, these values corresponding to the third set of data in Table I. The curve fits the left side of the "initial rise" (the hump above the Rutherford value) but does not fit the right side.

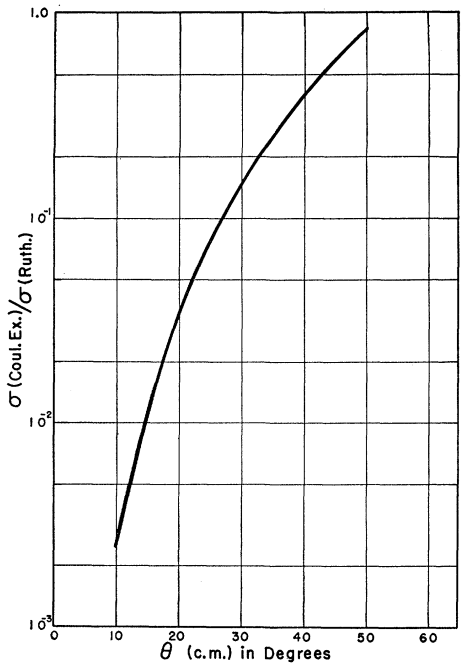

FIG. 8. The ratio of the electric quadrupole Coulomb excitation differential cross section to the Rutherford scattering cross section as a function of scattering angle for ($F^{19}+Tb^{159}$).

A fit to the right side of the rise can be obtained by decreasing the interaction radius R' by 3% (see second line in Table I); the lower curve in Fig. 10 shows the fit obtained. However, the left side of the hump is no longer fitted. The experimental "initial rise" for the $F^{19}+Tb^{159}$ scattering is therefore too wide to be fitted by the sharp-cutoff calculation in contrast to the fit obtained for the $O^{16}+Pb^{208}$ scattering. A difference in the scattering for the two experiments has thus been demonstrated.

D. Discussion of Experimental Results

The difference between the ($O^{16}+Pb^{208}$) and the ($F^{19}+Tb^{159}$) scattering data unfortunately cannot be used to draw unambiguous conclusions about the properties of the scattering interaction. This follows from the fact that in the ($F^{19}+Tb^{159}$) experiment

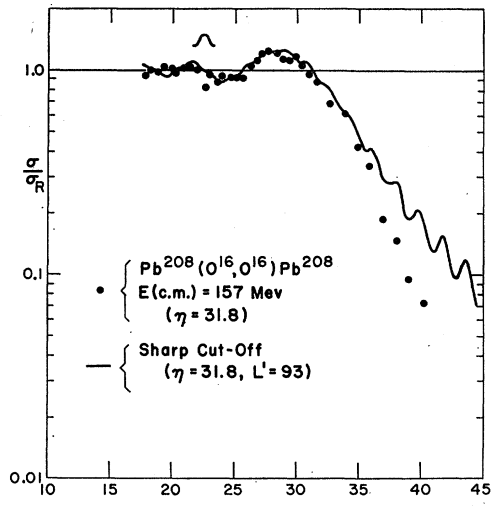

FIG. 9. Angular distribution obtained for the ($O^{16}+Pb^{208}$) scattering. The circles are experimental points; the curve is a calculated sharp-cutoff curve with $\eta=31.8$ and $L'=93$. The value for η is determined by the experimental conditions; the value for L' is adjusted so that the curve will fit the experimental data. The angular resolution is indicated by the Gaussian figure above the curve.

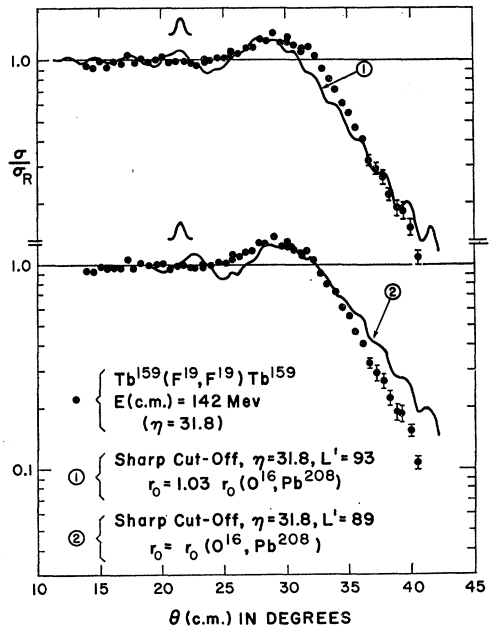

FIG. 10. Angular distribution obtained for the ($F^{19}+Tb^{159}$) scattering. The experimental points have been plotted twice for comparison to two sharp-cutoff curves. The value of η is the same for both curves, while L' is 93 for curve 1 and 89 for curve 2. These L' values correspond to r_0 values of 1.52×10^{-13} cm and 1.47×10^{-13} cm, respectively, with r_0 being related to R' by $R'=r_0\ (A^{\frac{1}{3}}+A'^{\frac{1}{3}})$. The angular resolution is indicated by the Gaussian figure above the curve.

inelastic scattering has been included with the elastic scattering. Nevertheless, because of the classical nature of the heavy-ion scattering ($\eta \sim 30$), it is possible to show that, to a first approximation, the angular distribution of the inelastically scattered ions should be the same as the angular distribution of the elastically scattered ions.

From the classical point of view, all ions passing by a point nucleus follow Rutherford scattering trajectories. Some of the ions interact with the nucleus through Coulomb excitation; these ions are the inelastically scattered ions. The remainder of the ions are the elastically scattered ions. Both inelastically and elastically scattered ions will follow essentially the same trajectories since the velocity of the inelastically scattered ion changes by only 0.1% because of the Coulomb excitation. Thus, classically, for a point nucleus the inelastic scattering cross section plus the elastic scattering cross section should equal the Rutherford scattering cross section, i.e., the sum of the inelastic and elastic cross sections should equal the true elastic cross section for a static (unexcitable) nucleus. For a nucleus of radius R' that is strongly absorbing for heavy ions, ions on trajectories passing inside of R' will be absorbed while those on more distant trajectories will be undisturbed. Again, from the classical viewpoint, both the elastically scattered and the inelastically scattered ions will be absorbed in the same fashion. Thus, an experiment measuring the sum of the elastic and inelastic scattering will measure the elastic scattering cross section that would be obtained from a static nucleus. Since the partial-wave analysis presented in Sec. II.A is based on the assumption of a static nucleus, the (F^{19}+Tb^{159}) experimental data which include both the inelastic and the elastic scattering should, from the classical point of view, be valid for analysis by the method of Sec. II.A.

However, the classical description of the scattering process is correct only to a first approximation. In particular, for trajectories passing near the nuclear surface, diffraction will occur because of the sharp transition from no absorption to strong absorption at the nuclear surface. And, these diffraction features would be expected to be considerably different for the inelastic scattering than for the elastic scattering. This expectation follows from the experience obtained with the scattering from light nuclei where diffraction features dominate. In these cases the electric quadrupole excitation of nuclei results in inelastic scattering angular distribution patterns almost exactly out of phase with respect to the elastic scattering angular distributions.[19] It is not clear therefore how significantly the inclusion of the inelastic scattering will modify the elastic scattering that occurs from a static nucleus; the classical features of the scattering predict a small modification, the quantum features a large modification.

[19] J. S. Blair, Phys. Rev. **115**, 928 (1959).

Some insight into the effect of the inelastic scattering has been obtained by making two tests. First, the assumption is made that the effect of the inelastic scattering is small. Then, partial-wave analyses of the (O^{16}+Pb^{208}) and the (F^{19}+Tb^{159}) scattering data can be made (neglecting such effects as spin-orbit coupling or nuclear distortion by polarization). The result of such analyses is to show a large difference between the scattering parameters L', ΔL_A, ΔL_δ, and $\delta_{L'}$ for the (O^{16}+Pb^{208}) and the (F^{19}+Tb^{159}) experiments. The conclusion then, subject to the assumptions made, is that there is a difference in the nuclear "surfaces" of Pb^{208} and Tb^{159}.

The second test was made with the cooperation of Dr. J. L. Yntema, Dr. B. Zeidman, and Dr. T. H. Braid of the Argonne National Laboratory who measured the elastic scattering of 43-Mev alpha particles by Pb^{208} and Tb^{159}. Since the Coulomb excitation cross section for electric quadrupole excitations has a ratio to Rutherford scattering varying approximately as E^3/Z' (E=c.m. energy and Z'=projectile charge number), the (He^4+Tb^{159}) inelastic scattering to elastic scattering ratio is reduced below the (F^{19}+Tb^{159}) ratio by $(42/142)^3/(2/9)=1/8.7$. This factor reduces the inelastic contribution to the alpha-particle scattering to a few percent of the elastic scattering so that the partial-wave analysis can be made with more assurance. Partial-wave analyses were made therefore for both (He^4+Pb^{208}) and (He^4+Tb^{159}). The result was that the same surface parameters ΔL_A, ΔL_δ, and $\delta_{L'}$ could be used to fit both sets of experimental data. Thus, the Pb^{208} and Tb^{159} "surfaces" are found to be the same according to alpha-particle scattering. This

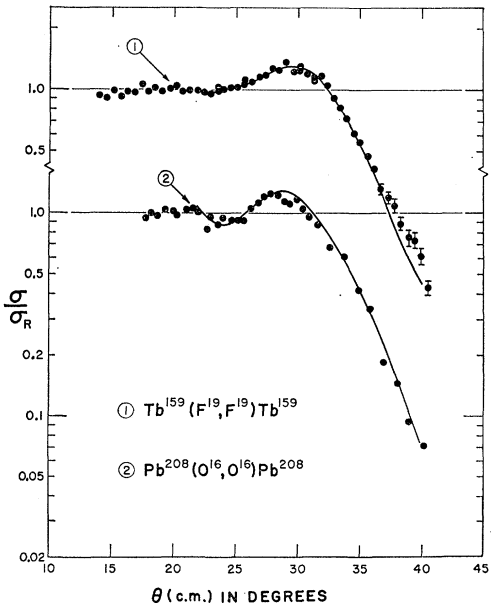

FIG. 11. The experimental data for (F^{19}+Tb^{159}) scattering and for (O^{16}+Pb^{208}) scattering fitted by curves calculated using a partial-wave analysis.

conclusion then implies that the experimental difference between the (O^{16}+Pb^{208}) and (F^{19}+Tb^{159}) scattering probably is not caused by surface effects. Rather the difference most likely is caused by either the inclusion of the inelastic scattering in the (F^{19}+Tb^{159}) experiment or by some other neglected effect such as the spin-orbit interaction or the deformation of the nucleus through polarization by the high-Z ion. A definite selection among these possibilities must await further experimental investigations.

In the following, a more complete account is presented of the calculations just discussed.

1. *Partial-Wave Analysis of the* O^{16} *and* F^{19} *Experiments*

Using the calculational procedure of Sec. II.A, values of L', ΔL_A, ΔL_δ, and $\delta_{L'}$ were determined that would yield σ/σ_R values agreeing with the (O^{16}+Pb^{208}) and (F^{19}+Tb^{159}) experimental data. The kind of fits obtained are shown in Fig. 11. The scattering "surface" parameters, ΔL_A, ΔL_δ, and $\delta_{L'}$, determined by these fits are shown in a three-dimensional plot in Fig. 12. The two "eggs," one for Pb and one for Tb, indicate the range of the variation in the scattering "surface" parameters that will give a satisfactory[20] fit to the experimental data. The projections of the eggs onto the three coordinate planes are also shown, to facilitate reading the values of the parameters. The important feature of Fig. 12 is that the two "eggs" are well separated which indicates that a different set of scattering "surface" parameters is required to describe the Pb and Tb scattering results. Therefore, if the inelastic scattering contribution to the (F^{19}+Tb^{159}) scattering does not distort the elastic scattering angular distribution, then the Tb^{159} "surface" would seem to be considerably "thicker" (ΔL_A and ΔL_δ larger) than the Pb^{208} "surface."

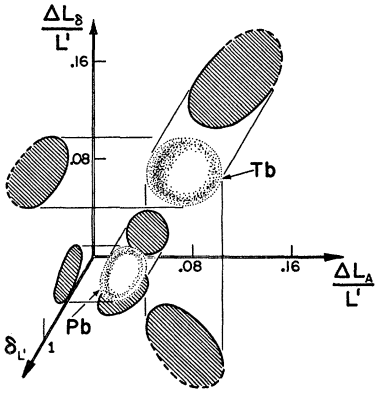

FIG. 12. A three-dimensional plot of the scattering "surface" parameters ΔL_A, ΔL_δ, and $\delta_{L'}$, determined by the partial-wave fits to the experimental data. Each "egg" determines the range of the scattering parameters that will give a satisfactory fit to the experimental data. For convenience in reading the boundary values of the "eggs," the "eggs" are also projected onto the three coordinate planes.

[20] The "satisfactory" fits were determined subjectively by examining curves such as those shown in Fig. 11.

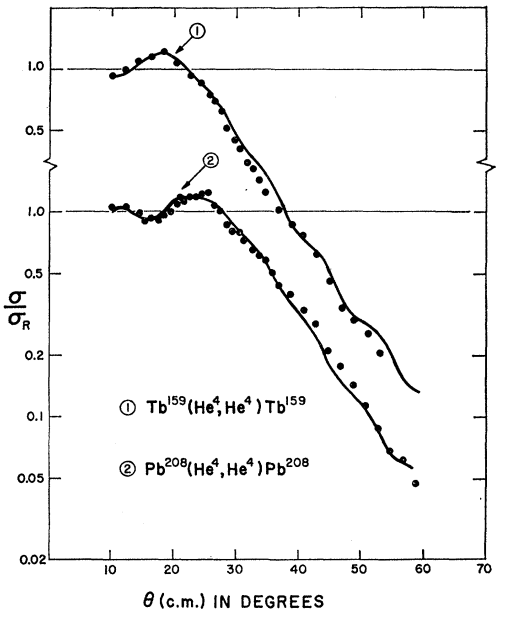

FIG. 13. The experimental data for (He^4+Tb^{159}) scattering and for (He^4+Pb^{208}) scattering fitted by curves calculated using a partial-wave analysis. The same values of the "surface" parameters ΔL_A, ΔL_δ, and $\delta_{L'}$ were used to fit both curves.

2. *Partial-Wave Analysis of the* He^4 *Experiments of Yntema, Zeidman, and Braid*

Using again the method of analysis outlined in Sec. II.A, the 43-Mev (He^4+Pb^{208}) and (He^4+Tb^{159}) experiments of Yntema, Zeidman, and Braid were fitted. The fits obtained are shown in Fig. 13. Except for L', the scattering parameters determined by the fits are the same for both Pb^{208} and Tb^{159}: $\Delta L_A=1.0$, $\Delta L_\delta=2.0$, and $\delta_{L'}=0.25$. The different L' values can be accounted for completely by the $A^{\frac{1}{3}}$ dependence of the nuclear radii. Therefore, the alpha-particle scattering data indicate that the "surfaces" of Pb^{208} and Tb^{159} are the same, in contradiction to the (O^{16}+Pb^{208}) and (F^{19}+Tb^{159}) experiments. Since the alpha-particle experiments do not include a significant amount of inelastic scattering due to Coulomb excitation, and the spin-orbit interaction and nuclear polarization are smaller than for the O^{16} and F^{19} experiments, the analysis for the alpha-particle experiments should be more reliable. Thus, the difference obtained with the heavier ions probably is not caused by a difference in the Pb^{208} and Tb^{159} surfaces, but rather is caused by some other effect such as inelastic scattering, spin-orbit interactions, or possibly nuclear deformation by the large charge of the high-Z projectile.

ACKNOWLEDGMENTS

Professor G. Breit has been most helpful in pointing out to us the limitations of the semiclassical approxi-

mation as well as the importance of the Coulomb excitation process. Professor G. H. Rawitscher and Professor J. S. McIntosh also have discussed with us the theoretical interpretation of the data. The experimental portion of this work has been greatly assisted by the work of J. Shuchatowitz on the evaporation of targets, K. Chung on the improvement of the resolution of the scintillation counter, A. Disco and J. Gill on the angle indicator, and D. Bates on the target positioning control. Finally, we wish to thank the accelerator crew under the direction of Dr. M. S. Malkin for the necessary heavy-ion beams.

PHYSICAL REVIEW VOLUME 125, NUMBER 2 JANUARY 15, 1962

Gamma Radiation from Proton Capture in Na^{23}†

F. W. PROSSER, JR., W. P. UNRUH, B. H. WILDENTHAL, AND R. W. KRONE
The University of Kansas, Lawrence, Kansas

(Received September 11, 1961)

The γ-ray decays of twelve resonances in the reaction $Na^{23}(p,\gamma)Mg^{24}$ in the proton energy range from 0.58 to 1.42 Mev have been re-examined with large scintillation detectors and coincidence techniques. A number of weaker cascades through the states of Mg^{24} between the excitation energies of 6 Mev and 8 Mev has been found. Relative intensities have been measured for the observed γ rays and consistent decay schemes proposed. The absolute yields of this reaction at these resonances have been determined.

INTRODUCTION

INCREASING interest in the collective interpretation of nuclear states in the nuclei of the $d_{\frac{5}{2}}$ shell[1,2] has prompted several recent investigations[3–5] of the states of Mg^{24}. A number of the states of intermediate excitation in Mg^{24} also are reached in the decay of various compound states observed in the $Na^{23}(p,\gamma)Mg^{24}$ reaction. Since most of the information on this reaction was obtained several years ago,[6–10] it was felt that a more thorough study, with the use of the multichannel analyzers and the larger scintillation crystals now available, would be of value. This paper will be primarily concerned with the assignment of relative intensities to the various γ rays observed and their incorporation into decay schemes at the resonances in this reaction between the bombarding energies of 0.58 and 1.42 Mev. Also, the absolute yield for γ-ray decay, $\omega\gamma$, of these resonances has been measured. The angular distributions and correlations of several of these γ rays will be discussed in a subsequent paper.

EXPERIMENTAL PROCEDURE

The electronics used in this study were standard. The γ radiation was detected with a 5-in. diam×5-in. thick NaI crystal mounted on a DuMont 6263 photomultiplier tube and the resulting pulse-height distributions were recorded on an RCL 256-channel analyzer. Where the complexity of the pulse height spectra required coincidence studies for confirmation of the proposed cascades, a 3-in. diam×3-in. thick NaI crystal was used as the second detector in a slow-fast coincidence circuit. The fast coincidence circuit consisted of four Hewlett-Packard Model 460AR amplifiers and an E-H Research Laboratories Model 101N coincidence analyzer with the resolving time set at 25 nsec. A slow coincidence between the fast-coincidence output and a window set on the desired portion of the spectrum from the 5-in.×5-in. detector gated the multichannel analyzer.

For most of the work and for the final assignment of relative intensities, the spectra were observed at an angle of 55° to the incident beam to minimize the effect of angular distributions on these assignments. To improve the effective resolution of the pulse height spectra, a 3-in. thick lead collimator was inserted between the target and the detector. The opening in the collimator was tapered to permit the passage of γ rays only in a cone which traversed the entire crystal. For the coincidence studies, the 5-in.×5-in. crystal was left at 55° with the collimator in place and the 3-in.×3-in. crystal was placed at about 80° to the beam on the opposite side of the target with its front face one inch from the target.

The targets were prepared by the evaporation of

† This work has been supported in part by the U. S. Atomic Energy Commission.

[1] H. E. Gove, *Proceedings of the International Conference on Nuclear Structure, Kingston*, edited by D. A. Bromley and E. W. Vogt (University of Toronto Press, Toronto, 1960), pp. 438–460.
[2] M. K. Banerjee, reference 1, pp. 461–463.
[3] C. Broude and H. E. Gove, reference 1, pp. 471–474.
[4] R. Batchelor, A. J. Ferguson, H. E. Gove, and A. E. Litherland, Nuclear Phys. **16**, 38 (1960).
[5] E. W. Hamburger and A. G. Blair, Phys. Rev. **119**, 777 (1960).
[6] F. W. Prosser, Jr., N. B. Baumann, D. K. Brice, W. G. Read, and R. W. Krone, Phys. Rev. **104**, 369 (1956).
[7] J. O. Newton, Phys. Rev. **96**, 241 (1954).
[8] F. C. Flack, J. G. Rutherglen, and P. J. Grant, Proc. Phys. Soc. (London) **A67**, 973 (1954).
[9] P. J. Grant, J. G. Rutherglen, F. C. Flack, and G. W. Hutchinson, Proc. Phys. Soc. (London) **A68**, 369 (1955).
[10] For a general bibliography of other reactions leading to Mg^{24}, see P. M. Endt and C. M. Braams, Revs. Modern Phys. **29**, 683 (1957), and *Nuclear Data Sheets* (National Academy of Sciences-National Research Council, Washington, D. C., 1960).